Synthesis of Fe_3O_4/α-Fe_2O_3/ZnO nanocomposite for antibacterial application

Cite as: AIP Conference Proceedings **2231**, 040031 (2020); https://doi.org/10.1063/5.0002472
Published Online: 22 April 2020

Vivian Saly Soplanit, Ahmad Taufiq, Arif Hidayat, et al.

Synthesis of Fe_3O_4/α-Fe_2O_3/ZnO Nanocomposite for Antibacterial Application

Vivian Saly Soplanit, Ahmad Taufiq*, Arif Hidayat, Ainun Nikmah, Defi Yuliantika, Habibatun Nurul Ulya, Rosy Eko Saputra

Department of Physics, Faculty of Mathematics and Natural Sciences, Universitas Negeri Malang, Jl. Semarang 5, Malang 65145, Indonesia

*Corresponding author: ahmad.taufiq.fmipa@um.ac.id

Abstract. Fe_3O_4 and α-Fe_2O_3 are potential magnetic materials to be developed in medical fields, especially for antibacterial agents. In order to support their application performance, Fe_3O_4 and α-Fe_2O_3 were combined with ZnO nanoparticles via an organic assisted route. The characterizations of Fe_3O_4/α-Fe_2O_3/ZnO nanocomposites were done employing FTIR, XRD, and SEM to study their functional groups, crystal structure, morphology, and particle distribution. The data analysis for infrared spectra presented that some peaks detected the presence of Fe3O4, α-Fe2O3, and ZnO at some positions. The phase composition for the Fe_3O_4, α-Fe_2O_3, and ZnO was respectively of 90.50%, 5.0%, and 4.5%. The SEM images showed that the Fe_3O_4/α-Fe_2O_3/ZnO nanocomposite tended to be constructed in spherical and plate shapes with the particle sizes of 12.25 ± 2.5 nm and 27.5 ± 2.5 nm, respectively. Furthermore, the antibacterial test presented that the Fe_3O_4/α-Fe_2O_3/ZnO nanocomposite had reasonable inhibition rate for *S. aureus*, *B. Subtilis*, and *E coli*.

INTRODUCTION

In the past five years, the development of nanocomposite-based materials has attracted many researchers. This is evidenced by the many reports related to the development of nanocomposite materials that are applied in various applications [1–3]. The researchers' interest in nanocomposite materials is generally associated with better physical or chemical properties compared to its precursor [4]. Technically, nanocomposite synthesis techniques combine two or more materials on a nanometer scale.

One material that is currently being developed as a precursor of nanocomposite materials is Fe_3O_4 (magnetite). Magnetite has advantages of non-toxic, excellent chemical stability, and superior resistance to high temperatures [5]. Furthermore, another magnetic material that is also widely studied related to the performance of its application in various fields is α-Fe_2O_3 (hematite). Meanwhile, ZnO is also a non-magnetic material that is also often compiled with magnetic material to improve the performance of the application.

Related to the use of nanocomposite techniques, ZnO is used as a filler in the system in this study to have more reliable bioactivity. The selection of ZnO is due to its relatively safe biocompatibility and biodegradation when applied in the medical field [6]. This study also used a template in the form of polyethylene glycol (PEG) with the aim of the resulting particles having a relatively smaller size [7]. Thus, this will improve the performance of the material when it is applied. Based on the advantages and prospects of the three precursors above, this study developed Fe_3O_4/α-Fe_2O_3/ZnO nanocomposite particles as candidates for an antibacterial material.

International Conference on Life Sciences and Technology (ICoLiST)
AIP Conf. Proc. 2231, 040031-1–040031-7; https://doi.org/10.1063/5.0002472
Published by AIP Publishing. 978-0-7354-1990-2/$30.00

EXPERIMENTAL DETAILS

Synthesis of $Fe_3O_4/\alpha\text{-}Fe_2O_3/ZnO$ Employing Coprecipitation Method

Iron sand was extracted by a separation method using permanent magnets. The pure iron sand was dissolved in HCl and stirred with a magnetic stirrer at a constant speed of 720 rpm at room temperature for 30 minutes to obtain a brown solution. The solution was then titrated with NH_4OH at room temperature for 30 minutes. After the process, the resulting solution was washed repeatedly with aqua dest until it reaches a pH of 7. Afterward, the solution was filtered using filter paper to obtain a wet precipitate. PEG solution was prepared by dissolving in H_2O and sterilizing at a speed of 720 rpm at 90 $^{\circ}$C. The precipitated wet precipitate was added to the PEG solution, which had been dissolved and stirred using a magnetic stirrer. Then, the solution was filtered so that Fe_3O_4/PEG was deposited and dried at 100 $^{\circ}$C, and a magnetic powder sample was obtained. Synthesis of ZnO nanoparticles was carried out by applying zinc acetate dihydrate with water and stirring using a magnetic stirrer at room temperature. The pH of the solution was adjusted to pH 13, utilizing a solution for 60 minutes to obtain a solution. The reaction solution was washed with methanol and filtered to dry at 100 $^{\circ}$C for 1 hour. In the final process, Fe_3O_4-PEG nanoparticle powder was dissolved into 150 ml DI Water. Stirred using an ultrasonic machine for 30 minutes at room temperature. Additionally, the reaction solution was added with zinc acetate dihydrate and sterilized for 30 minutes. After that, the pH of the solution was adjusted to pH 10 using 5 M NH_4OH, and then both were inserted for 30 minutes using a magnetic stirrer. The resulting solution was deposited then washed using ethanol and DI Water. After the washing process, the precipitate was filtered with filter paper and then dried at 750 $^{\circ}$C for 2 hours to obtain $Fe_3O_4/\alpha\text{-}Fe_2O_3/ZnO$ powder.

Characterization Method

A series of characterization of $Fe_3O_4/\alpha\text{-}Fe_2O_3/ZnO$ samples was carried out to obtain elemental, structural, morphological**,** and functional groups as fundamental studies before being applied as antimicrobial agents. The characterization was carried out using X-ray diffraction (XRD), Fourier-transform infrared spectroscopy (FTIR), and scanning electron microscopy (SEM). Furthermore, the antibacterial activity of the material was carried out through the agar diffusion method against three different types of bacteria. The identification of antibacterial activity was reviewed based on the diameter of the inhibited zone obtained.

RESULTS AND DISCUSSION

Functional Group of $Fe_3O_4/\alpha\text{-}Fe_2O_3/ZnO$ Nanocomposite

The functional groups of $Fe_3O_4/\alpha\text{-}Fe_2O_3/ZnO$ were tested using Fourier-transform infrared spectroscopy (FTIR). FTIR test results are presented in Fig. 1. Based on the analysis results, the sample is confirmed by the formation of the absorption peak at the wavenumber around 400-4000 cm^{-1}. The identification peak of Fe-O absorption at wavenumbers 552 cm^{-1} and 447 cm^{-1} peaks of Zn-O absorption was observed. The appearance of these two peaks signifies the success of the composite formation. This is in line with research conducted by Saffari *et al*. (2015), which identified the presence of Fe-O and Zn-O uptake around 565 and 435 cm^{-1} [8]. Other absorption bands were also detected at 3471, 1620, and 1041 cm^{-1}, identifying the presence of vibrations from O-H and indicating a stretch of water molecules in the sample [9–11]. The characteristic of the formation of PEG in the sample is marked by the presence of C-O bonds in the absorption band 1097-1197 cm^{-1}. Another absorption band from PEG was also detected in 1866 and 2010 cm^{-1}, indicating the presence of COC- and CH_2 bonds [9,12]. Uniquely, the PEG functional groups in this sample were not detected. This is associated with a PEG melting point of no more than 100 $^{\circ}$**C** [13]. Thus, if the sample is treated, the high sintering process causes the PEG function group to disappear.

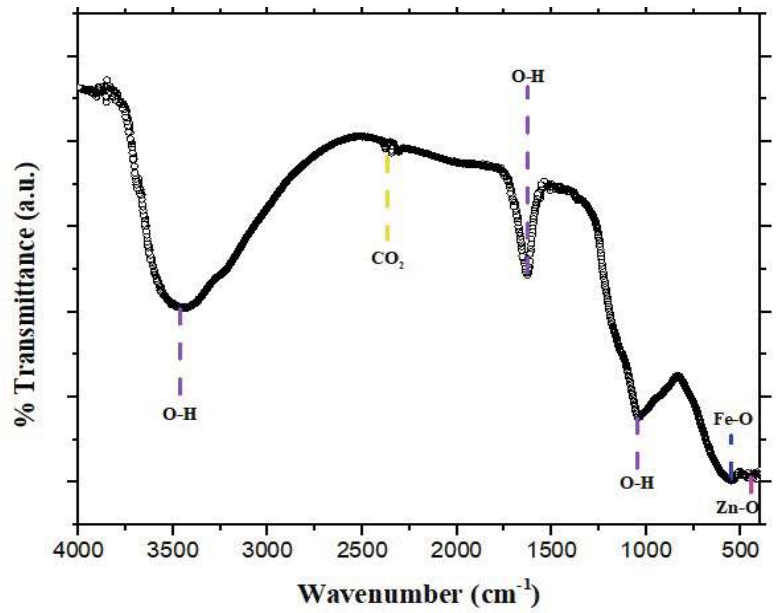

FIGURE 1. Function group of $Fe_3O_4/\alpha\text{-}Fe_2O_3/ZnO$ nanocomposite

Crystal Structure of $Fe_3O_4/\alpha\text{-}Fe_2O_3/ZnO$ Nanocomposite

The XRD pattern was analyzed using X-ray diffraction in the range of 2-teta 20°-80° and with the wavenumber Cu-Kα (λ = 1.54 Å). XRD characterization was carried out, aiming to determine the crystal structure, phase, and grain size in the sample. The type of material can be determined by comparing the results of XRD characterization with existing models. Fig. 2 presents the result of the analysis of diffraction pattern data from $Fe_3O_4/\alpha\text{-}Fe_2O_3/ZnO$ nanocomposite.

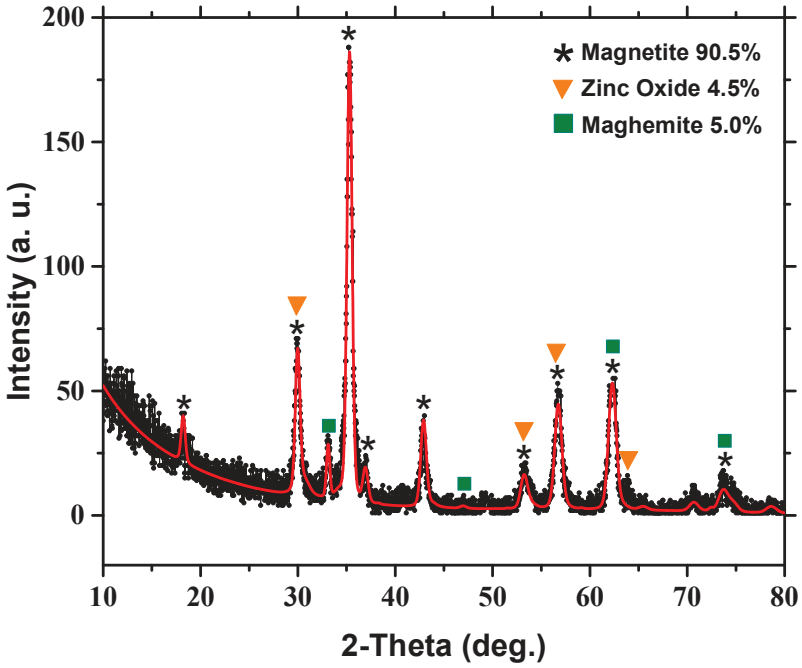

FIGURE 2. XRD diffraction pattern of $Fe_3O_4/\alpha\text{-}Fe_2O_3/ZnO$ nanocomposite

The results of the XRD analysis in Fig. 2 shows that in the diffraction pattern of $Fe_3O_4/\alpha\text{-}Fe_2O_3/ZnO$ nanocomposite, identified 3 phases appear, namely Fe_3O_4, ZnO, and $\alpha\text{-}Fe_2O_3$ phases. Based on the analysis of the diet, these peaks appear following AMCSD data no. 0007766 for the Fe_3O_4 model, AMCSD no. 0005204 for ZnO and AMCSD no. 0018106 for $\alpha\text{-}Fe_2O_3$. The emergence of the phase informs that the sample at a temperature sintering treatment of 750 °C forms the $Fe_3O_4/\alpha\text{-}Fe_2O_3/ZnO$ nanocomposite. However, the single, hematite phase ($\alpha\text{-}Fe_2O_3$) is also formed as a result of high-temperature treatment. This phase arises due to the influence of high sintering temperatures that cause crystal structure defects [14]. Crystal structure changes due to the position of the atoms that change with increasing temperature, so the structure of the atoms that are formed are getting stronger. The dominant percentage of the Fe_3O_4 phase causes the peak of ZnO nanoparticle diffraction to sink. This is consistent with the theory, the higher the sintering temperature used, the higher the crystallinity of Fe_3O_4 [15]. This shows that the $Fe_3O_4/\alpha\text{-}Fe_2O_3/ZnO$ nanocomposite with 750 °C sintering temperature treatment causes the Fe_3O_4 phase to be more dominant, with a percentage reaching 90.50%.

TABLE 1. XRD analysis results of $Fe_3O_4/\alpha\text{-}Fe_2O_3/ZnO$ nanocomposite using the Rietveld method

Crystal Parameter		**A peak of- (2-Teta)**
Magnetite (Fe_3O_4)		
a = *b* = *c* (Å)	8.42	(1) 18.26°; (2) 30.04°
Crystal size (nm)	19.32	(3) 35.37°; (4) 36.95°
Phase percentage	90.50	(5) 42.84°; (6) 53.15°
Bragg R-factor	9.96	(7) 56.77°; (8) 62.44°; (9) 73.65°
Zinc Oksida (ZnO)		
a = *b* (Å)	3.40	(1) 30.04°
c (Å)	5.78	(2) 53.94°
Crystal size (nm)	9.37	(3) 56.77°
Phase percentage	4.50	(4) 64.62°
Bragg R-factor	11.11	
Maghemite ($\alpha\text{-}Fe_2O_3$)		
a = *b* (Å)	5.41	(1) 33.22°
c (Å)	5.43	(2) 45.22°
Crystal size (nm)	32.81	(3) 62.44°
Phase percentage (%)	5.00	(4) 74.33°
Bragg R-factor	11.81	
Refinement Parameter		
Rp	19.27	
RwP	23.35	
GoF (%)	1.41	

To find out the crystal structure of Fe_3O_4, ZnO, and $\alpha\text{-}Fe_2O_3$, the VESTA software shown in Fig. 3 can be used. Besides, particle size and lattice parameters resulting from the software analysis are shown in Table 1. The crystal structure of Fe_3O_4 in Fig. 3 (a) is an inverse cubic spinel with an Fd3m space group. This system informs that Fe^{2+} ions occupy all octahedral parts, and the other half is occupied by Fe^{3+} ions, while tetrahedral parts are filled by Fe^{3+} ions [3]. Fig. 3 (b), Visualization of ZnO crystal structure showing the existence of two interconnected submissions, including Zn^{2+} and O^{2-}, so that each Zn ion is surrounded by tetrahedral ions and vice versa [16]. Fig. 3 (c) is a crystal structure owned by $\alpha\text{-}Fe_2O_3$ (hematite) in the form of Rhombohedral with R3C space group. In this crystal structure, Fe^{3+} ions occupy two-thirds of the octahedral sites bounded by hexagonal close-packed O grids. [17].

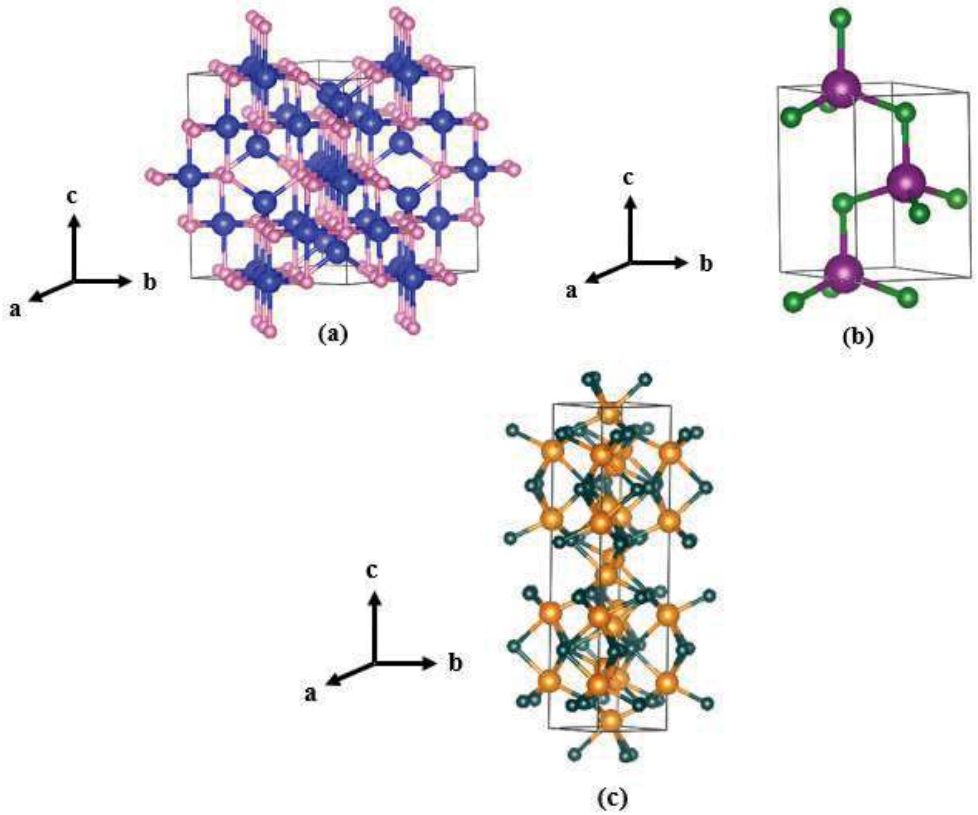

FIGURE 3. Crystal structure (a) Fe_3O_4 nanoparticle, (b) ZnO nanoparticle, (c) α- Fe_2O_3 nanoparticle

Morphology and Size Distribution of Fe_3O_4/α-Fe_2O_3/ZnO Nanocomposite

Fig 4 presents the surface morphology and size distribution of Fe_3O_4/α-Fe_2O_3/ZnO nanocomposite. Based on Fig. 4a can be observed that the sample has spherical morphology; this is related to the growth of crystals in the samples that form agglomeration due to sintering temperature treatment [15]. Another effect of the 750 ˚C sintering temperature is the dominance of the ZnO phase with sheet-shaped morphology. The formation of the morphology of ZnO nanoparticles resembling sheets is caused by the interaction of charged poles between particles, which causes the particles to experience strain force and size effect-oriented to a particular field [18,19].

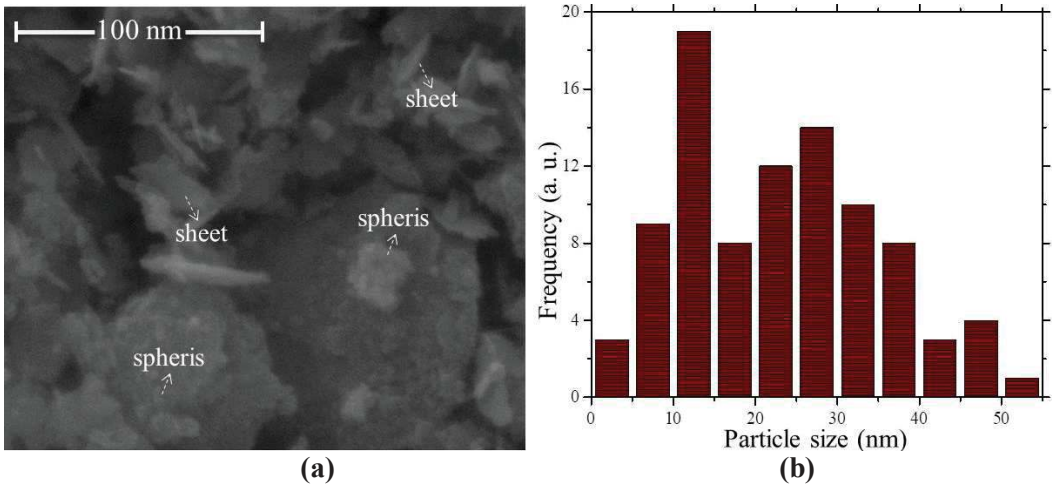

FIGURE 4. (a) SEM image and (b) particle size distribution of Fe_3O_4/α-Fe_2O_3/ZnO nanocomposite

This different morphology causes the size distribution of $Fe_3O_4/\alpha\text{-}Fe_2O_3/ZnO$ nanocomposite particles to vary. From the results of the analysis of the size distribution in Fig. 4b, it is known that the most substantial particle size frequency is in the range of 12.5 ± 2.5 nm and 27.5 ± 2.5 nm. Nanoparticles with spherical morphology had an average particle size of 12.5 ± 2.5 nm, while particles with sheet morphology dominated the size of 27.5 ± 2.5 nm. The results of the analysis of SEM nanoparticles with XRD showed the corresponding results. In the research, the synthesized $Fe_3O_4/\alpha\text{-}Fe_2O_3/ZnO$ nanocomposite has nanospheres and nanosheet morphology due to high-temperature treatment.

Antibacterial Activity of $Fe_3O_4/\alpha\text{-}Fe_2O_3/ZnO$

Observed in Fig. 5 samples showed inhibition against microorganisms, the inhibitory sample for *S. aureus* bacteria was 1.57 mm, for *B. subtilis* bacteria was 5.95 mm, and the inhibitory power for *E. Coli* bacteria was 6.4 mm. The inhibitory power of the sample against bacterial growth is related to reactive oxygen species (ROS) in the sample, which causes damage to proteins and DNA [20,21]. The addition of ZnO in the composite system supports the inhibition of samples against bacteria. Some researchers claim that ZnO also has excellent antibacterial properties and shows a broad spectrum of antibacterial growth because it can produce H_2O_2 or superoxide due to the existence of paired electron holes [22,23]. Nanocomposites help in separating and reducing bacterial growth through an external magnetic field [24]. ZnO can produce hydroxyl radicals (• OH), which will play a role in killing bacteria [25].

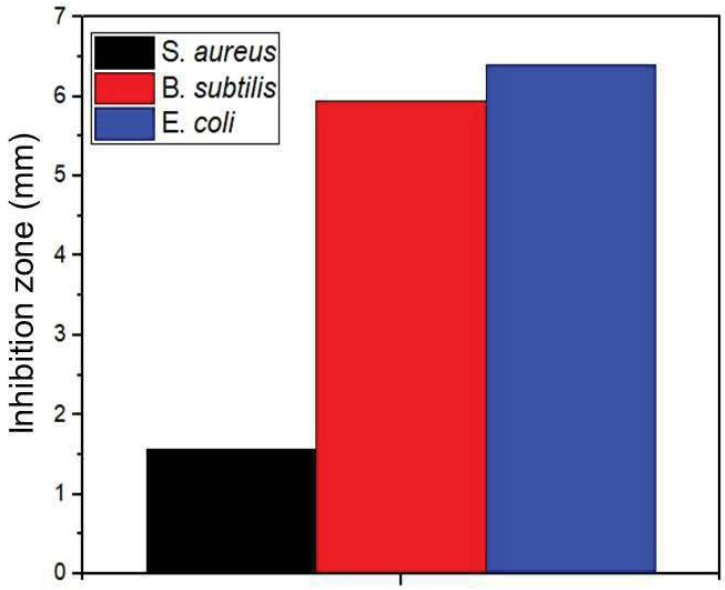

FIGURE 5. Antibacterial activity of $Fe_3O_4/\alpha\text{-}Fe_2O_3/ZnO$ nanocomposite

SUMMARY

The $Fe_3O_4/\alpha\text{-}Fe_2O_3/ZnO$ nanocomposite was successfully synthesized using the coprecipitation and sol-gel method. The function group of $Fe_3O_4/\alpha\text{-}Fe_2O_3/ZnO$ nanocomposite results from FTIR analysis showed that the PEG compound was not detected in the sample due to the sintering temperature treatment. Analysis of the crystal structure using the Rietveld method shows that the Fe_3O_4 phase has an inverse spinel cubic structure with a crystal size of 19.32 nm while ZnO has a hexagonal structure with a 9.37 nm crystal size where this corresponds to the results of SEM analysis. The impurity phase is $\alpha\text{-}Fe_2O_3$ with rhombohedral structure and 32.81 nm particle size. The $\alpha\text{-}Fe_2O_3$ phase in SEM analysis results has a morphology that resembles a plate while the $Fe_3O_4/\alpha\text{-}Fe_2O_3/ZnO$ nanocomposite has spherical morphology. Furthermore, concerning the application, the antibacterial analysis showed that the $Fe_3O_4/\alpha\text{-}Fe_2O_3/ZnO$ nanocomposite had a sample inhibition of S. aureus bacteria of 1.57 mm, for *B. Subtilis* bacteria of 5.95 mm and inhibition of *E. Coli* bacteria of 6.4 mm.

ACKNOWLEDGMENTS

Our sincere thanks are addressed to Universitas Negeri Malang (UM) for the research funding through PNBP scheme.

REFERENCES

1. F. Fajaroh, S. Marfu'ah, and A. Nur, in *Journal of Physics: Conference Series* (IOP Publishing, 2018), p. 012022.
2. D.K. Padhi, T.K. Panigrahi, K. Parida, S.K. Singh, and P.M. Mishra, ACS Sustainable Chemistry & Engineering **5**, 10551 (2017).
3. P. Qin, C. Chen, Y. Wang, L. Zhang, and P. Wang, Journal of Nanoscience and Nanotechnology **17**, 9350 (2017).
4. M. Miculescu, V.K. Thakur, F. Miculescu, and S.I. Voicu, Polymers for Advanced Technologies **27**, 844 (2016).
5. P.N.V.K. Pallela, S. Ummey, L.K. Ruddaraju, S. Gadi, C.S. Cherukuri, S. Barla, and S.V.N. Pammi, Heliyon **5**, e02765 (2019).
6. J. Jiang, J. Pi, and J. Cai, Bioinorganic Chemistry and Applications **2018**, (2018).
7. A. Taufiq, F.N. Ikasari, D. Yuliantika, S. Sunaryono, N. Mufti, H. Susanto, E. Suarsini, N. Hidayat, A. Fuad, and A. Hidayat, Materials Today: Proceedings **17**, 1728 (2019).
8. J. Saffari, N. Mir, D. Ghanbari, K. Khandan-Barani, A. Hassanabadi, and M.R. Hosseini-Tabatabaei, Journal of Materials Science: Materials in Electronics **26**, 9591 (2015).
9. A. Roychowdhury, S.P. Pati, A.K. Mishra, S. Kumar, and D. Das, Journal of Physical and Chemistry of Solids **74**, 811 (2013).
10. A. Habibi-Yangjeh and M. Shekofteh-Gohari, Separation and Purification Technology **184**, 334 (2017).
11. A. Ahmed, D. Latif, and W. 'a Abdulridha, 2016 (2016).
12. K. Zomorodian, H. Veisi, M. Mousavi, M. Ataabadi, S. Yazdanpanah, M.J. Bagheri, A. Mehr, S. Hemmati, and H. Veisi, International Journal of Nanomedicine **Volume 13**, 3965 (2018).
13. V. Wiesmet, E. Weidner, S. Behme, G. Sadowski, and W. Arlt, The Journal of Supercritical Fluids **17**, 1 (2000).
14. J.A. Morales-Morales, Ciencia En Desarrollo **8**, 99 (2017).
15. T.Y. Rozi and A. Astuti, Jurnal Fisika Unand **5**, 351 (2016).
16. T. Dalgleish, J.M.G.. Williams, A.-M.J. Golden, N. Perkins, L.F. Barrett, P.J. Barnard, C. Au Yeung, V. Murphy, R. Elward, K. Tchanturia, and E. Watkins, Journal of Experimental Psychology: General **136**, 23 (2007).
17. W. Wu, Z. Wu, T. Yu, C. Jiang, and W.-S. Kim, Science and Technology of Advanced Materials **16**, 023501 (2015).
18. N. Pattanayak, A. Bhattacharyya, S. Chakravarty, and A. Bajpai, Journal of Physics: Condensed Matter **31**, 365802 (2019).
19. A. Umar and Y.B. Hahn, Nanotechnology **17**, 2174 (2006).
20. X. Pan, J.E. Redding, P.A. Wiley, L. Wen, J.S. McConnell, and B. Zhang, Chemosphere **79**, 113 (2010).
21. N.B. Saleh, B. Chambers, N. Aich, J. Plazas-Tuttle, H.N. Phung-Ngoc, and M.J. Kirisits, Frontiers in Microbiology **6**, 677 (2015).
22. S. Baruah, S. K Pal, and J. Dutta, Nanoscience & Nanotechnology-Asia **2**, 90 (2012).
23. P. Goyal, S. Chakraborty, and S.K. Misra, Environmental Nanotechnology, Monitoring & Management **10**, 28 (2018).
24. S. Singh, K.C. Barick, and D. Bahadur, Journal of Materials Chemistry A **1**, 3325 (2013).
25. A. Lipovsky, Y. Nitzan, A. Gedanken, and R. Lubart, Nanotechnology **22**, 105101 (2011).